

Article

Numerical Study of Inclination Effect of the Floating Solar Still Fitted with a Baffle in 3D Double Diffusive Natural Convection

Mohammed A. Almeshaal¹ and Chemseddine Maatki^{1,2,*}

¹ Department of Mechanical Engineering, College of Engineering, Imam Mohammad Ibn Saud Islamic University, Riyadh 11432, Saudi Arabia

² Laboratory of Metrology and Energy Systems, National Engineering School, Energy Engineering Department, University of Monastir, Monastir 5000, Tunisia

* Correspondence: casmaatki@imamu.edu.sa

Abstract: A three-dimensional computational study of double-diffusive natural convection was conducted to explore the impact of tilt on the thermal and solutal performance of a floating pyramidal solar still filled with an air-steam mixture. In the present work, the still is cooled from the upper walls and is maintained at a low vapor concentration. The bottom wall of the still is maintained at a hot temperature and high concentration. Four different models of baffles placed in the upper region of the solar still have been studied. The mathematical formulation of the equations governing the problem is based on the vector current potential-vorticity formalism. The numerical method of finite volumes is used. The effect of Rayleigh and tilt angle of the floating solar still on the flow structure, iso-temperatures, iso-concentrations, and heat and mass transfer rates were examined. The most relevant results of this study are (i) an uncooled air-vapor mixture outlet was observed during tilting for the solar still equipped with a small, flat baffle, (ii) triangular and curvilinear baffle configurations are suitable to guide the air-vapor mixture towards the cold walls during the tilting of the solar still floating on the sea, and (iii) the triangular baffle configuration is the most relevant design, enhancing thermal and solutal performance by 20%.



Citation: Almeshaal, M.A.; Maatki, C. Numerical Study of Inclination Effect of the Floating Solar Still Fitted with a Baffle in 3D Double Diffusive Natural Convection. *Processes* **2022**, *10*, 1607. <https://doi.org/10.3390/pr10081607>

Academic Editors: Tereza Kudelova and Erik Bartuli

Received: 29 June 2022

Accepted: 9 August 2022

Published: 13 August 2022

Publisher's Note: MDPI stays neutral with regard to jurisdictional claims in published maps and institutional affiliations.



Copyright: © 2022 by the authors. Licensee MDPI, Basel, Switzerland. This article is an open access article distributed under the terms and conditions of the Creative Commons Attribution (CC BY) license (<https://creativecommons.org/licenses/by/4.0/>).

Keywords: 3D numerical analysis; double-diffusive convection; solar still; heat and mass transfer; pyramid shape; inclination; baffle

1. Introduction

The pressure on water resources in several regions of the world is increasing every day. Highly vulnerable to the effects of climate change, many countries have already opted for the mobilization of unconventional resources: the desalination of seawater or brackish water despite the relatively high costs of these operations. To overcome this crisis, researchers have been careful to develop new desalination methods and devices using renewable energy sources, such as solar energy, and the solar still device is one of them. Due to its simplicity and low cost of operation and maintenance, several studies and research have been conducted to develop and improve the efficiency of solar stills.

The majority of the reviewed research focuses on performance improvement based on the design and development of different geometries and configurations of solar stills. The most studied designs of solar stills are rectangular solar stills (Ghachem et al. [1]), concave wick solar stills (Sathyamurthy, et al. [2]), tubular stills, triangular stills (Rahbar et al. [3]), and pyramid-shaped stills (Al-Madhhachi et al. [4] and Moussa and Hatem [5]). Abdelgaied [6] studied the pyramidal shape using an absorbent graphite plate and cooling the glass cover. They observed an improvement in daily efficiency of 98.9% compared to a traditional pyramidal still. Other researchers have proposed improvements to the condensing surface of the still. Jianyin Xiong et al. [7] investigated numerically and experimentally the multi-effect solar desalination with a stacked and corrugated plate condensing surface. They observed that when the departure temperature is fairly high, the global efficiency of

the desalination equipment reaches 91%. R. Dev and G. N. Tiwari [8] studied the different slopes of condensation cover in summer and winter. They found that 45° tilted passive solar offered the best efficiency for both seasons. The authors also examined different water depths, they found that a shallow water depth gives better efficiency.

Owing to its advantages represented by the land economy and environmental sustainability, offshore floating solar stills have become an important stage of research and development in recent years. However, the instability in real weather conditions limits its application. Sebastian et al. [9] investigated the influence of different parameters, such as internal relative humidity, vapor space temperature, and glass lid temperature, on the performance of a three-layer multipurpose floating absorber solar still. They found that relative humidity and vapor space temperature negatively affect the productivity of the modified solar still during afternoon hours. Kaushal et al. [10] experimentally compared the performance of the multi-effect vertical diffusion still with floating wicks and waste heat recovery to that of the reference still in the same meteorological and operating conditions. They found that the distillate productivity was 21% higher than that of the reference still. Ni et al. [11] experimentally studied a floating solar still rejecting salt using the concept of interfacial solar heat localization. The evaporation zone of the designed solar still is composed of black fabric, under which is an insulating structure that simultaneously serves to thermally insulate the evaporation layer and reject excess salts into the water below. They obtained a daily yield of 1.29 kg/m²/day. Although the freshwater yield of floating solar panels was significantly improved in their study, it is still much lower than that of land-based solar panels. Wang et al. [12] studied the design of a solar still with a floating solar desalination film that uses concentrated light. The authors performed an optical simulation of the light concentration process and examined the heat and mass transfer. They observed that the water production per unit area of this test system reached 1.38 kg/m²/day. Chen et al. [13] studied the seawater supply to a bionic floating solar still inspired by the water uptake of plant roots. The authors observed a decrease in downward heat loss and uniformity of water uptake. They obtained a daily freshwater yield of 1.5 kg/m²/day.

Within a passive solar still, salt or brine absorbs heat from the bottom of the still to warm up. As time passes, the water temperature rises and drives the evaporation of water molecules. Convection is produced in the air over the surface of the water, drawing the molecules of water vapor upward. When air is saturated with vapor and contacts the cold surface of the cover glass, there is condensation of some water vapor molecules. The air-vapor mixture is the medium between the evaporating surface and the condensing surface of the solar still. The flow of the air-vapor mixture through a solar still is governed by the phenomenon of natural double diffusion convection. Several research studies have studied the natural double-diffusive convection in solar stills. Alvarado-Juárez et al. [14] numerically investigated natural double-diffusive convection and thermal surface radiation in a tilted rectangular cavity simulating a solar still. The authors found that the surface thermal radiation shifts the flow of the fluid from a single-cell to a multi-cell model and raises the velocity closer to the walls. They also showed that the Nusselt number and Sherwood number increased by 25% and 15%, respectively. The numerical study of natural double-diffusive convection in a tilted rectangular cavity, which simulates a solar still, is performed by Alvarado-Juárez et al. [15]. They analyzed the effect of aspect ratio and inclination angle by varying the Rayleigh number between 9×10^4 and 6×10^6 . They observed that when the aspect ratio decreases, the multicellular pattern decreases, and the convective heat and mass transfer increases up to 41%. They also showed that as the inclination angle rose, the Sherwood and Nusselt numbers increased up to 3.8%. A computational study of three-dimensional double-diffusive natural convection in a tilted rectangular solar still has been established by Ghachem et al. [16]. The effects of buoyancy ratio and cavity inclination are investigated. They showed that as N increases, a reversal of the main flow rotation occurs, resulting in an increasing dominance of the solute over the thermal thrust. They also showed that the maximum of Nusselt and Sherwood numbers occurs at an angle of 30° to the horizontal. Recently, Maatki [17] has numerically studied

the triangular solar still and proposed an improvement of the evaporation surface. By increasing the number of feeder connections, the author showed an improvement in the performance of the solar still.

Although baffles have often been used to suppress natural convection in enclosures, the literature also shows that their appropriate placement enhances natural convection and could potentially improve the performance of solar stills. Subhani and Kumar [18] numerically examined the effect of natural convection induced by a constant and variable thermal gradient on the condensing and evaporating surfaces with and without a baffle on a single slope solar still. They studied the positioning of the baffle on the left side of the still. They showed that the presence of the baffle halfway up the left wall improves the heat transfer rate on the evaporating surface side. Edalatpour et al. [19] numerically investigated the two-dimensional natural convection heat transfer in a single slope solar still with baffles. They showed that the use of a single baffle can significantly increase the system performance compared to multiple baffles. Serradj et al. [20] examined the effect of vertically mounted passive baffles on natural convection in a single slope solar still. The authors numerically studied the effect of the length and position of the baffles on the stills. They showed that the baffles increase the natural convection heat transfer coefficient by 20%.

The objective of this work is to study the effects of tilting, i.e., the inclination of the floating solar still equipped with baffles and filled with an air-vapor mixture, on the thermal and mass ratios in natural double diffusion convection. Indeed, the variations of the metrological conditions generating waves in a rough sea affect the stability of the floating distiller by tilting it during its operation. The thermal and mass performances are thus disturbed. The novelty in this work is the study of the effect of the design of the baffle installed in the upper region of the solar still as well as the tilt angle of the floating solar still on the flow structure, thermal, and mass performances.

2. Physical Model and Governing Equations

2.1. Physical Model

The model of the floating solar still filled with an air-vapor mixture considered in this work is shown in Figure 1a. The geometry is pyramidal, with a maximum height, H , from the base surface to the top, and a square base surface of dimension, H . The solar still consists of two zones, the lower zone being considered the heating zone and the upper zone as the cooling zone. Between these two zones, thin baffles of dimensions $L \times H$ are installed.

Figure 1b shows the pyramidal solar still which is designed to float on the surface of the salt water, absorb and convert the incident solar flux into thermal energy, and transfer this heat to the saltwater below for steam production. The angle of inclination θ of the floating solar still is defined in reference to the horizontal sea level.

The pyramidal cavity is filled with an air-vapor mixture defined by $Le = 0.85$ and $Pr = 0.7$. The bottom wall is composed of two impermeable sections and three permeable sections with the highest vapor concentration ($C' = C'_h$) and temperature ($T' = T'_h$). The upper walls inclined at an angle of 45° to the horizontal, model the glazed cover with external cooling, having a lower vapor concentration ($C' = C'_c$) and temperature ($T' = T'_c$).

Figure 1c–f illustrates the four different designs of baffles studied. The baffles consist of thin symmetrical glass panels having the width of the still and are attached to the vertical walls of the solar still at a fixed height of $(0.4 \times H)$ from the bottom surface and are designed to collect the cooled fluid, considered as distillate, from the inclined cooling surfaces and to direct it to the outlet. The distillate is discharged through a window with a height of $0.1 \times H$ having the same width as the solar still and located on the two vertical walls just above the baffles. They are considered permeable walls. Case 0 is a flat baffle of length $L_1 = 0.1 \times H$, case 1 is flat also of length $L_2 = 0.3 \times H$, and cases 2 and 3 have the same length as case 2 and are triangular and curvilinear, respectively. The other walls (vertical walls and distillate collection panels) are considered adiabatic and impermeable.

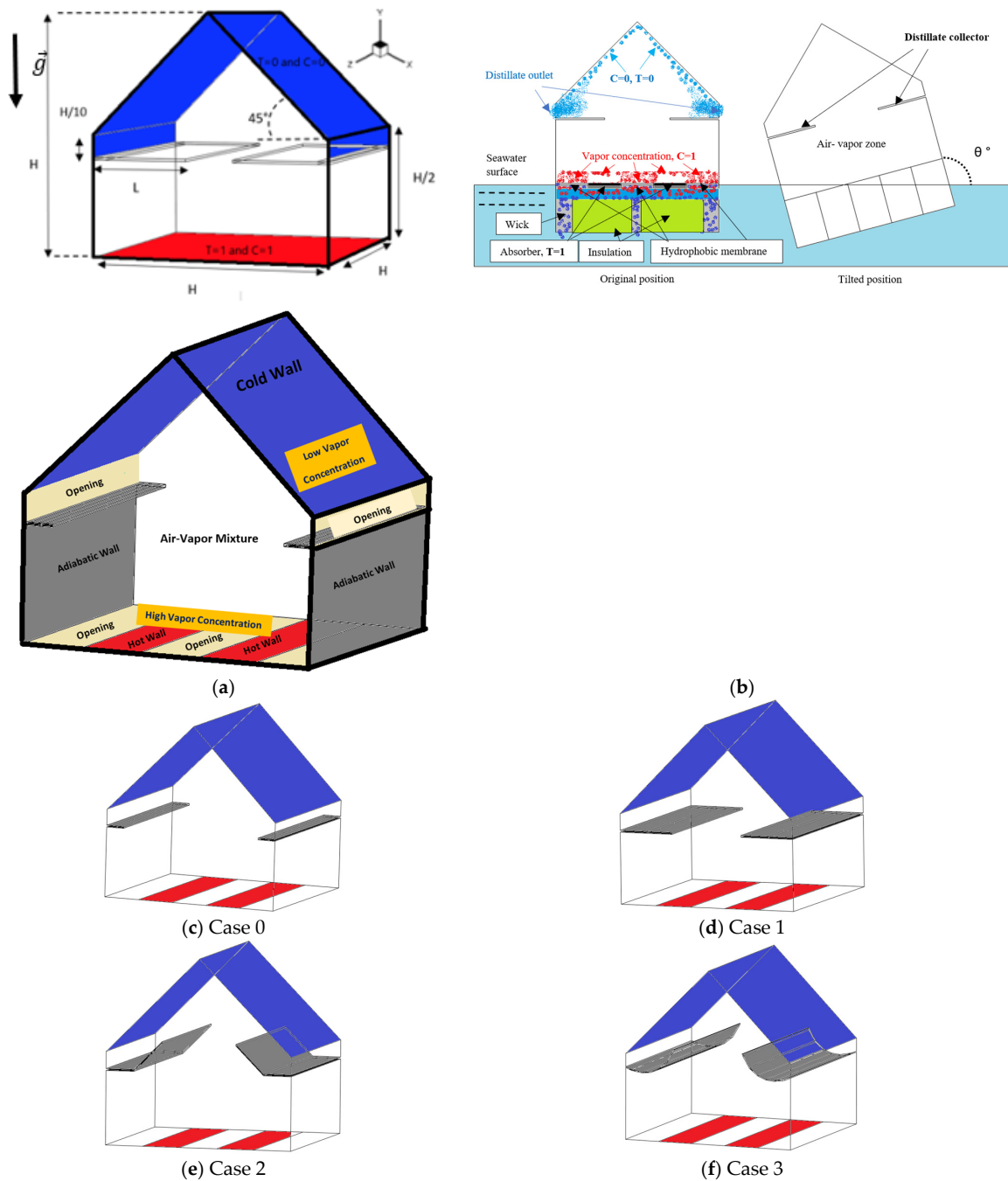


Figure 1. Physical Models and different designs of baffles studied. (a) shows the model of the floating solar still filled with an air-vapor mixture considered in this work; (b) shows the pyramidal solar still which is designed to float on the surface of the salt water, absorb and convert the incident solar flux into thermal energy, and transfer this heat to the saltwater below for steam production; (c–f) illustrates the four different designs of baffles studied.

2.2. Governing Equations, Assymtions, and Boundary Conditions

The fluid, a vapor-air mixture, is assumed to be Newtonian and incompressible. The flow is considered to be laminar and the Soret and Dufour effects are ignored. Heat transfer by radiation is neglected. All other thermo-physical properties of the air-vapor mixture are supposed to be constant. The Boussinesq approximation was used for the fluid density. The density varies linearly with temperature and concentration according to the following relationship:

$$\rho = \rho_0 [1 - \beta_T(T' - T_0) - \beta_C(C' - C_0)] \quad (1)$$

where T' is the temperature of the fluid and C' is the concentration of water vapor at a given point in the solar still. ρ_0 , T_0 , and C_0 are density, temperature, and concentration at reference, respectively. β_T and β_C represent the thermal and mass expansion coefficients.

In this work, it is assumed that the flow of the air-vapor fluid mixture is governed by laminar double-diffusive natural convection without phase change. It is assumed also that the vapor is already generated by the bottom wall. The governing equations of the examined solar still model, are written using the three-dimensional potential-vorticity vector formulation ($\vec{\psi} - \vec{\omega}$) that suppresses the pressure gradient [1,21].

Considering all assumptions, the conservation equation of mass, momentum, energy, and concentration are written in the following vector form:

$$\nabla \vec{V}' = 0 \quad (2)$$

$$\frac{\partial \vec{V}'}{\partial t'} + (\vec{V}' \times \nabla) \vec{V}' = -\frac{1}{\rho_0} \nabla P' + \nu \Delta \vec{V}' + [1 - \beta_T(T' - T_0) - \beta_C(C' - C_0)] \vec{g} \quad (3)$$

$$\frac{\partial T'}{\partial t'} + \vec{V}' \times \nabla T' = \alpha \Delta T' \quad (4)$$

$$\frac{\partial C'}{\partial t'} + \vec{V}' \times \nabla C' = D \Delta C' \quad (5)$$

The stated governing equations were then given in dimensionless form as:

$$-\vec{\omega} = \nabla^2 \vec{\psi} \quad (6)$$

$$\frac{\partial \vec{\omega}}{\partial t} + (\vec{V} \cdot \nabla) \vec{\omega} - (\vec{\omega} \cdot \nabla) \vec{V} = \Delta \vec{\omega} + Ra.Pr. \begin{bmatrix} -\left(\frac{\partial T}{\partial z} - N \frac{\partial C}{\partial z}\right) \sin \theta \\ \left(\frac{\partial T}{\partial z} - N \frac{\partial C}{\partial z}\right) \cos \theta \\ \left(\frac{\partial T}{\partial x} - N \frac{\partial C}{\partial x}\right) \sin \theta + \left(-\frac{\partial T}{\partial y} + N \frac{\partial C}{\partial y}\right) \cos \theta \end{bmatrix} \quad (7)$$

$$\frac{\partial T}{\partial t} + \vec{V} \cdot \nabla T = \nabla^2 T \quad (8)$$

$$\frac{\partial C}{\partial t} + \vec{V} \cdot \nabla C = \frac{1}{Le} \nabla^2 C \quad (9)$$

where $Ra = \frac{g\beta_i(T'_h - T'_c)H^3}{\alpha\nu}$, $Le = \frac{\alpha}{D} = \frac{Sc}{Pr}$, $Pr = \frac{\alpha}{\nu}$, and $N = \frac{\beta_c(C'_h - C'_l)}{\beta_i(T'_h - T'_c)}$. These respectively defined non-dimensional numbers are Rayleigh number, Lewis number, Prandtl number, and buoyancy ratio.

C'_h and C'_l are the high and low concentrations. T'_h and T'_c are the hot and cold temperatures.

Dimensionless variables employed in this study are $(x, y, z) = \frac{(x', y', z')}{H}$, the dimensionless temperature and concentration are $T = \frac{T' - T'_c}{T'_h - T'_c}$, $C = \frac{C' - C'_l}{C'_h - C'_l}$ and the dimensionless velocity and time are: $(u_x, u_y, u_z) = \frac{(u'_x, u'_y, u'_z)H}{\alpha}$ and $t = \frac{t'}{\alpha H^2}$.

The boundary conditions for:

- Concentration and temperature: $C(x, 0, z) = 1$, $T(x, 0, z) = 1$.

On the walls, when $y \geq 0.4$: $C(x, y, z) = 0$ and $T(x, y, z) = 0$, and $\frac{\partial T}{\partial n} = 0$ and $\frac{\partial C}{\partial n} = 0$ on other walls.

- Velocity: $u_x = u_y = u_z = 0$ on all walls.

At the open boundary: When $y = 0$, $\frac{\partial u_x}{\partial y} = \frac{\partial u_y}{\partial y} = \frac{\partial u_z}{\partial y} = 0$.

When $0.4 \leq y \leq 0.5$, $\frac{\partial u_x}{\partial x} = \frac{\partial u_y}{\partial x} = \frac{\partial u_z}{\partial x} = 0$.

- Vorticity and vector potential:

Vorticity: $\omega_x = 0, \omega_y = -\frac{\partial u_z}{\partial x}, \omega_z = \frac{\partial u_y}{\partial x}$ at $x = 0$ and $1, \omega_x = \frac{\partial u_z}{\partial y}, \omega_y = 0, \omega_z = -\frac{\partial u_x}{\partial y}$ at $y = 0$ and $1, \omega_x = -\frac{\partial u_y}{\partial z}, \omega_y = \frac{\partial u_x}{\partial z}, \omega_z = 0$ at $z = 0$ and 1 .

- Vector potential: $\frac{\partial \psi_x}{\partial x} = \psi_y = \psi_z = 0$ at $x = 0$ and $1, \psi_x = \frac{\partial \psi_y}{\partial y} = \psi_z = 0$ at $y = 0$ and $1, \psi_x = \psi_y = \frac{\partial \psi_z}{\partial z} = 0$ at $z = 0$ and 1 .

The average Nusselt and Sherwood numbers are given, respectively as:

$Nu_{av} = \int_0^1 \int_0^1 Nu \cdot \partial x \cdot \partial z$ and $Sh_{av} = \int_0^1 \int_0^1 Sh \cdot \partial x \cdot \partial z$, where Nu and Sh are the local Nusselt and local Sherwood numbers, and are expressed by:

$$Nu = \frac{\partial T}{\partial y} \Big|_{y=0,1}; Sh = \frac{\partial C}{\partial y} \Big|_{y=0,1}.$$

3. Numerical Method, Validation, and Grid Sensitivity

3.1. Numerical Method

The finite volume methodology was adopted to discretize the governing differential equations of problems (6–9). The power scheme is taken to handle the convection-diffusion terms [22]. The time-step is set to 10^{-4} .

The steps for solving the numerical code algorithm are as follows:

- Step 1: Initializing;
- Step 2: Resolution of the energy equation;
- Step 3: Resolution of the concentration equation
- Step 4: Resolution of the vorticity equation;
- Step 5: Resolution of the potential vector equation.

Steps 2 through 5 were then repeated until a convergence criterion was met. The iterated solution is running up to convergence at each time step. The convergence is reached once the maximized residues of the governing equations of the control grid volume are below 10^{-5} .

The blocked-off region method was used in this study to model the pyramidal solar still with different designs of the baffles [22,23]. The blocked-off region method involves sketching a rectangular domain surrounding the physical domain of concern. By that procedure, the domain is partitioned into two regions: active and non-active or blocked regions. This approach allows the use of algorithms that are applied in the regular geometries, for irregular geometries, which include sloping or curving boundaries [22]. Through this method, the sloped and curvilinear surfaces in the present study are approximated by a series of fine cubic steps, Figure 2. The use of fine grids in the interface region between the active and inactive areas results in an approximated boundary that is closer to the real boundary.

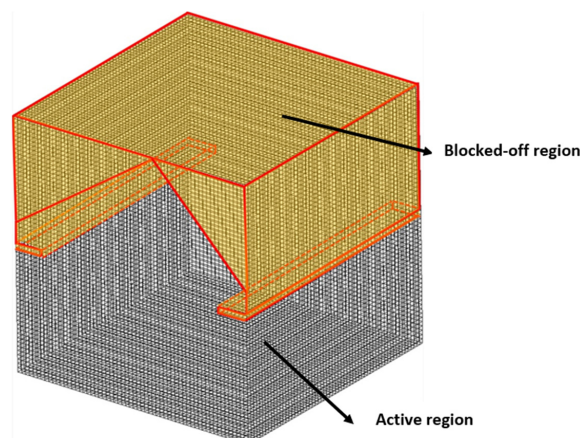


Figure 2. Blocked-off region in a regular grid.

3.2. Validation

The comparison between the results of the average Nusselt and Sherwood numbers computed by our numerical code and the results of Rahman et al. [24] for ($Le = 2$, $Pr = 0.7$, and $N = 1$) in a trapezoidal-shaped cavity at 30° angle is displayed in Figure 3. The result of the comparison revealed excellent agreement between both results, showing a deviation below 0.8% for all Grashof number values.

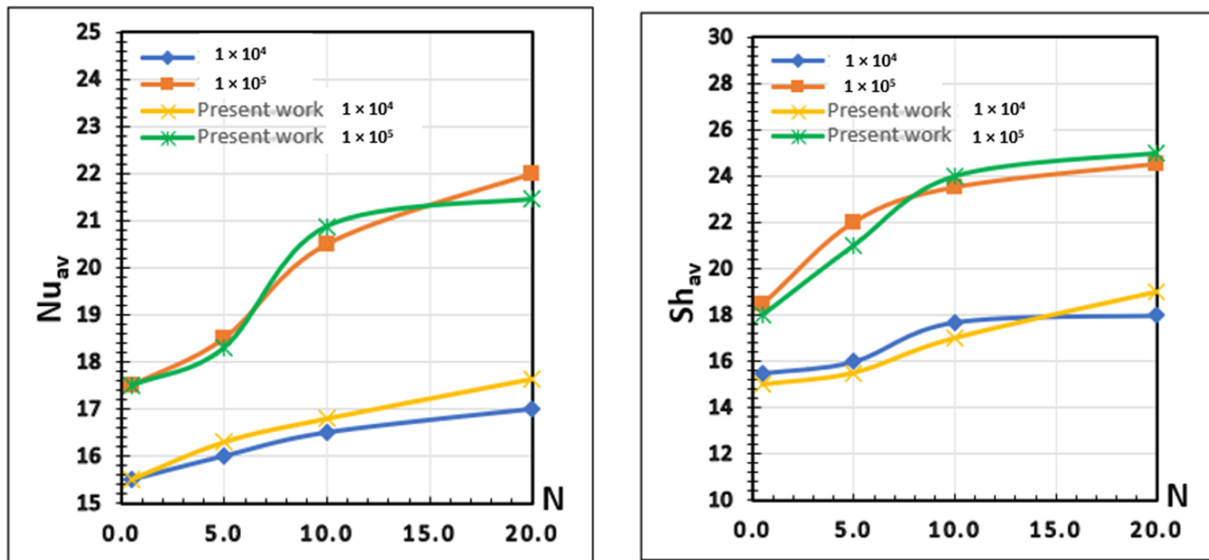


Figure 3. Comparison between the results of the average Nusselt and Sherwood numbers in the current study with the results of Rahman et al. [24].

3.3. Grid Sensitivity

The sensitivity of the grid presented in Table 1, is conducted for case 0, $N = 0$, and $Ra = 10^4$. Four distinct mesh sizes were checked (41^3 , 51^3 , 61^3 , and 71^3). The average Sherwood number is taken as the sensible variable. The incremental rise in Sh_{av} between grid sizes 61^3 and 71^3 is about 0.14%. Hence, by considering the economy of computation and accuracy, a 61^3 mesh size is used.

Table 1. Grid sensitivity test for case 0, $N = 0$ and $Ra = 10^4$.

Mesh Size	Sh_{av}	Percentage Increase	Incremental Increase
41^3	2.697	-	-
51^3	2.733	1.33481646	-
61^3	2.854	5.82128291	4.48646644
71^3	2.8578	5.9621802	0.14089729

4. Results and Discussion

The flow of the air-water vapor mixture in the solar still is governed by the natural double-diffusive convection phenomenon. To investigate the effect of inclination on the thermal and solutal performance of a pyramid-shaped floating solar still filled with the air-vapor mixture ($Le = 0.85$ and $Pr = 0.7$), four different configurations of baffles mounted in the upper region of the cavity, cooling region, have been studied. Case 0, considered as a reference case, is a flat baffle with length $L_1 = 0.1 \times H$, case 1 is also flat with length $L_2 = 0.3 \times H$, cases 2 and 3 have the same length as case 2 and are triangular and curvilinear respectively. A mixture of air and water vapor is assumed to be perfect and the flow is laminar. Rayleigh numbers between $10^3 \leq Ra \leq 5 \times 10^4$ and a positive buoyancy ratio between $0 \leq N \leq 2$ are considered in the computations. All thermo-physical properties of the air vapor are taken as constant. The tilt angles are in the range of $0^\circ \leq \theta \leq 25^\circ$ with an

increment of 5°. The results of the three-dimensional numerical study of double-diffusive convection in the floating solar still are presented in the patterns of streamlines, particle trajectories, iso-temperatures, and iso-concentrations, Nusselt and Sherwood averages.

4.1. Flow Structure, Iso-Temperatures, and Iso-Concentrations

In this section, the analysis and discussion of the flow structure of the air-vapor mixture, iso-concentration, and iso-temperature will be based on a comparison with the most efficient flow in a solar still.

In our physical model, it is assumed that steam is already generated from the bottom wall. The bottom wall is composed of two impermeable sections and three permeable sections with the highest concentration and temperature. The cavity, the subject of the study, is filled with an air-vapor mixture. The sloping walls at the top of the cavity are cold and have the lowest vapor concentration.

Due to the thermal and mass gradient, double-diffusive convection governs the flow. Thus, the fluid mixture naturally enters through the impermeable walls, heats up near the hot sections of the bottom wall, rises due to buoyancy forces acting on the density of the mixture and comes into contact with the cold inclined walls, falls back down cold near the adiabatic side walls and exits through the open windows.

Figure 4 shows the particle trajectory, temperature, and concentration iso-surfaces for buoyancy ratio $N = 0$ at different Rayleigh values in the reference case, case 0 in the initial position ($\theta = 0^\circ$).

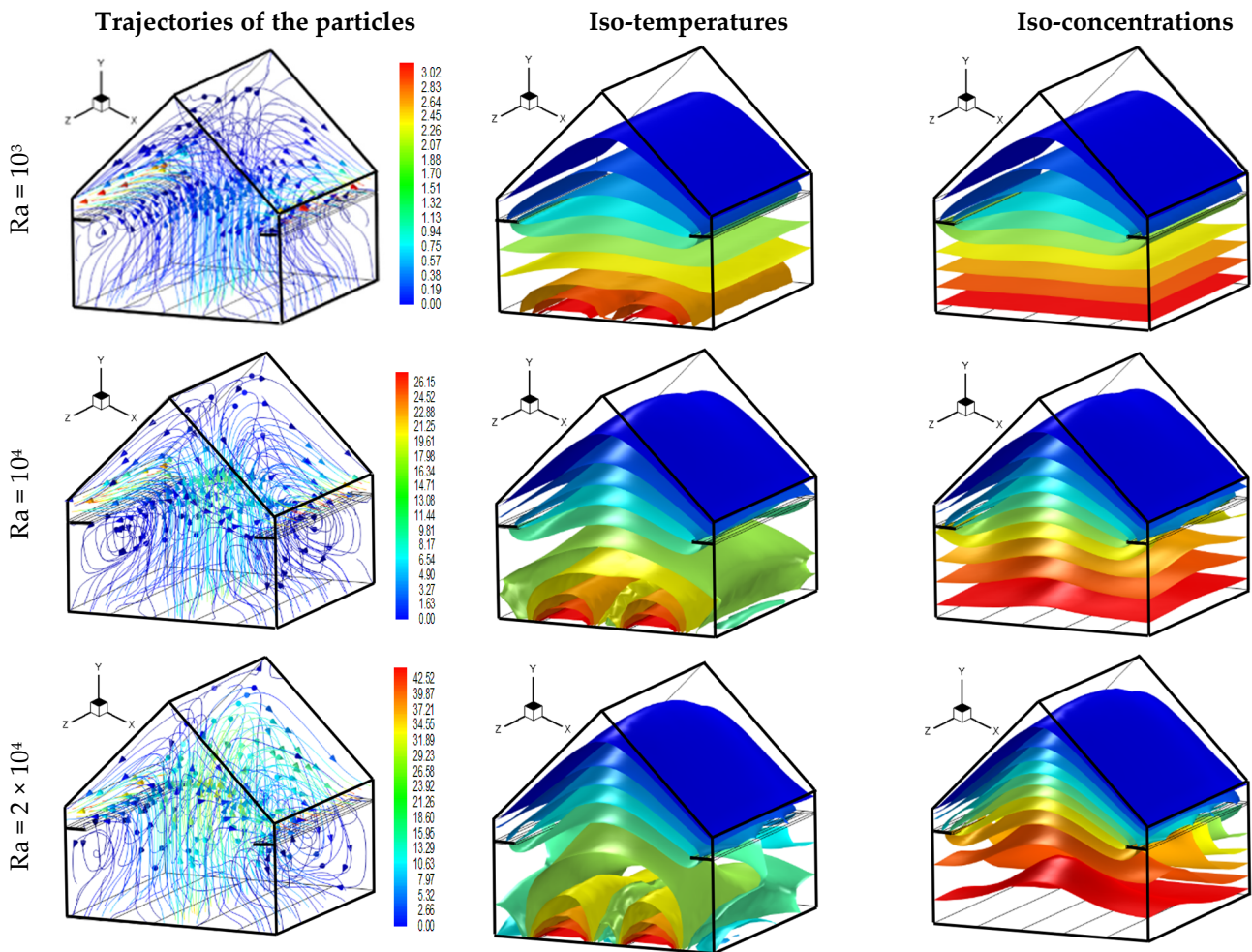


Figure 4. Particle trajectories, iso-surfaces of temperature and concentration for $N = 0$ and $\theta = 0^\circ$ (case 0)

When $Ra = 10^3$, the flow strength is weak, and the thermal and mass buoyancy forces do not allow the fluid to reach the cold walls. In this case, the fluid escapes directly from the outlet windows by pressure gradient without being cooled.

The temperature iso-surfaces show a horizontal stratification throughout the cavity. The thermal gradients are small on both the hot and cold surfaces. The concentration iso-surfaces show a dominant diffusive regime at this Rayleigh number. When Ra increases to 10^4 , the intensity of the flow increases, in fact, the maximum velocity increases from 3.02 to 26.15. The development of two symmetrical vortices rotating in opposite directions is observed slightly below the baffles. The two vortices have a three-dimensional character by spiral effect. The temperature iso-surfaces show the transition to the convective mode. Thermal gradients increase at the bottom and top of the cavity. A slight attenuation of the horizontal stratification of the concentration iso-surfaces is observed. The concentration gradient increases mainly near the cold surfaces. When $Ra = 2 \times 10^4$, the flow becomes three-dimensional mainly in the upper region of the cavity, the vapor cooling region. The two vortices below the baffles decrease in size but increase in intensity. The temperature iso-surfaces show the dominance of convective effects. The shape of the temperature iso-surfaces becomes parabolic throughout the cavity. The thermal gradients are intensified near the active walls. The structure of the concentration iso-surfaces highlights the significance of the three-dimensional character of the flow. Mass convection becomes increasingly intense at this Rayleigh number.

Figure 5a shows the effect of the tilt of the floating solar still in operating condition on the flow structure at the $z = 0.5$ plane. When $Ra = 10^3$ and $\theta = 5^\circ$, the flow structure shows an asymmetric flow of air-vapor mixture from the base surface to the cooling surfaces. Two small vortices are developed under the baffles. The particle trajectories show that there is a leakage of the uncooled air-vapor mixture to the right distillate outlet window. When $\theta = 15^\circ$, the right vortex disappears while the left one expands. A quantity of hot air-vapor mixture located in the right part of the cavity is trapped in the lower zone and no longer reaches the cooling zone. At $\theta = 25^\circ$, the vortex expands more and more and occupies the central part of the cavity. The cooling of the mixture becomes essentially localized at the left cold surface. A slight rise in flow intensity is observed with increasing tilt angle. When $Ra = 5 \times 10^4$, the transition from $\theta = 5^\circ$ to $\theta = 15^\circ$ is characterized by the appearance of a vortex rotating counter-clockwise at the left central zone of the cavity. The maximum intensity of the velocity increases.

Moving to $\theta = 25^\circ$, the flow intensity decreases and the developed vortex takes the central area of the cavity. The air-vapor trapping in the right zone noticed disappears at $Ra = 10^3$, but an uncooled air-vapor leakage is still observed from the right distillate outlet window.

Figure 5b illustrates the tilt effect of the floating solar still on the concentration iso-surfaces in the $z = 0.5$ plane. When $Ra = 10^3$, the concentration iso-surfaces exhibit a dominant diffusive regime. Increasing cavity tilt indicates a slight variation in the solutal gradient at the bottom surface. When $Ra = 5 \times 10^4$ and $\theta = 5^\circ$, the concentration iso-surfaces show a higher solutal gradient on the left side of the low wall compared to the right side. While it is higher on the right side of the cooling zone. The concentration iso-surfaces have a slightly inclined parabolic shape. At $\theta = 15^\circ$ and 25° , the iso-concentration structure is S-shaped in the central region of the cavity. The solutal gradients increasingly rise near the left and right low cooling active walls at $\theta = 25^\circ$. While the solutal gradient decreases near the left cooling wall.

Figure 5c presents the tilt effect of the floating solar still on the temperature iso-surfaces in the $z = 0.5$ plane. The cavity tilt has no remarkable effect on the iso-temperature structure when $Ra = 10^3$. The conductive regime is dominant. When $Ra = 5 \times 10^4$, at $\theta = 5^\circ$, the temperature iso-contours form parabolic patterns surrounding the hot impermeable surfaces. When passing to $\theta = 15^\circ$, the left thermal gradient of the cold wall decreases. At $\theta = 25^\circ$, the thermal gradient at both cold surfaces decreases significantly.

The effect of the shape of the baffles on the particle trajectory in the $z = 0.5$ plane for $\theta = 15^\circ$ is shown in Figure 6a. For the reference case shown in Figure 6a ($\theta = 15^\circ$ and $Ra = 10^3$), the particle trajectory shows uncooled air-vapor leakage to the distillate outlet window on the right and vortex development on the left. At this Rayleigh number, the three types of baffles designs presented in Figure 6a, show the absence of this vortex development. The particle trajectory for case 1, also shows uncooled air-vapor leakage to the distillate outlet window on the right. This problem disappears in cases 2 and 3. When $Ra = 5 \times 10^4$, the flow structure in case 1 is characterized by the development of two vortices near the left baffle. The maximum velocity, in this case, is lower than in the reference case. In cases 2 and 3, the flow structure is characterized by a single vortex and the maximum velocity intensity decreases further. It is noted also that the maximum velocity intensity is minimal in case 2. The shape of the baffles in cases 2 and 3 assisted the air-vapor mixture to cool before the exit.

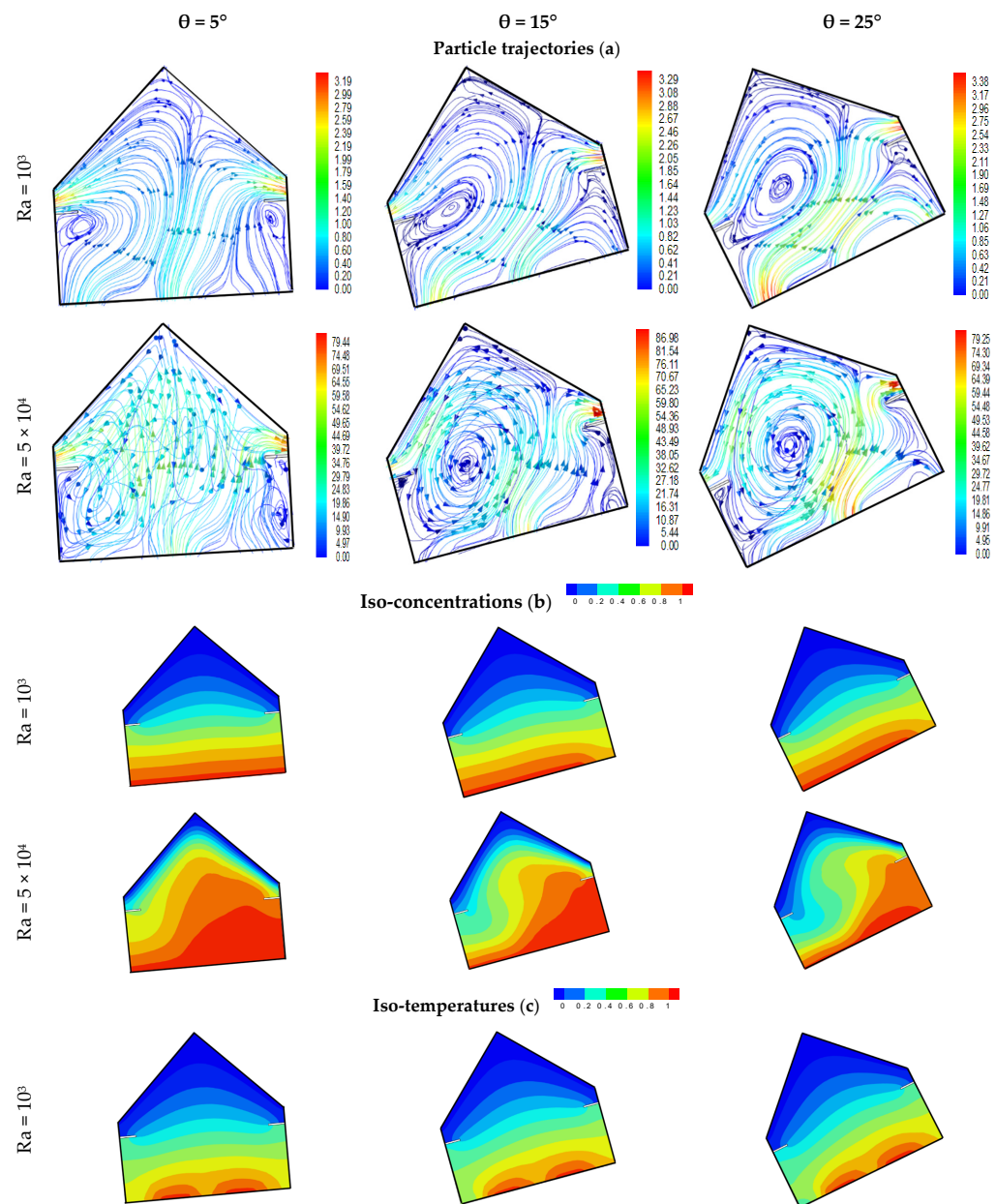


Figure 5. Cont.

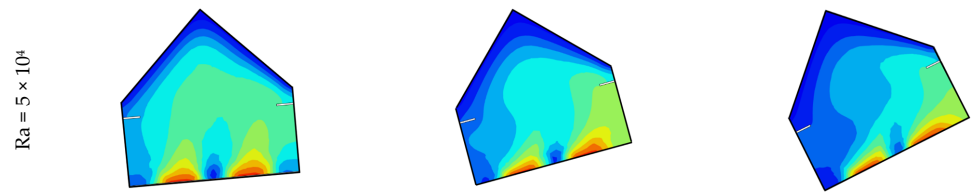


Figure 5. Particle trajectories (a), iso-contours of concentration (b) and temperature (c) for $N = 0$ and $z = 0.5$ (case 0).

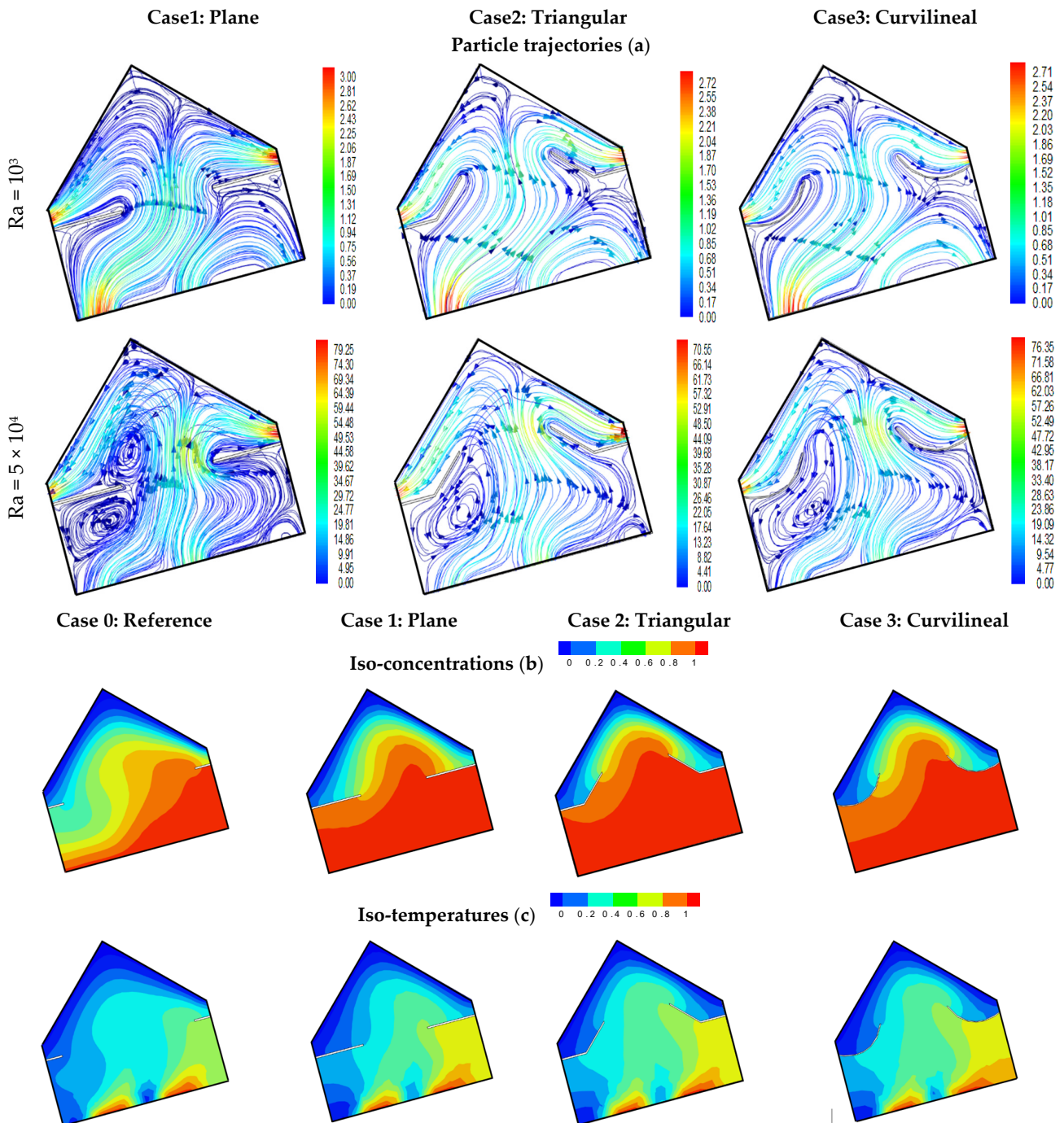


Figure 6. Particle trajectories (a), Iso-concentration (b) and iso-temperature (c), for $z = 0.5$ $N = 0$, $\theta = 15^\circ$ and $Ra = 5 \times 10^4$.

Figure 6b illustrates the effect of baffle shape on iso-concentration at $\theta = 15^\circ$ and $Ra = 5 \times 10^4$. In the reference case, the air-vapor convection takes an upward movement from the right zone with a high solutal gradient in the lower left part of the cavity. However, in cases 1, 2, and 3, the air-vapor convection is almost uniformly in the lower part of the solar still. The solutal gradient in the cooling zone has decreased in cases 2 and 3 compared to the reference case at this Rayleigh number. An improvement of the air-vapor convection is observed in the heating zone for all the new baffle designs studied.

Figure 6c presents the effect of baffle shape on iso-temperature at $\theta = 15^\circ$ and $Ra = 5 \times 10^4$. The temperature iso-contours show that the thermal gradient has decreased in the lower part of the cavity in cases 1, 2, and 3. On the other hand, the impact of thermal convection in the central part of the cavity is improved. The thermal gradient is enhanced in the cooling zone mainly in the middle of the cold surfaces for cases 2 and 3.

4.2. Heat and Masse Transfer Rates

Figure 7a presents the impact of the Rayleigh number on the heat transfer rate for $N = 0.5$ and $\theta = 0^\circ$. The average heat transfer rate is doubled when the Rayleigh number passes from $Ra = 10^3$ to 10^4 , showing a shift from the conductive to the convective regime for all cases studied. An improvement of 50% is observed when the Rayleigh number is moved from 10^4 to 5×10^4 . Case 2 shows that the heat transfer rate is maximum for $Ra = 2 \times 10^4$. While for $Ra = 5 \times 10^4$, case 3 shows the maximum heat transfer rate.

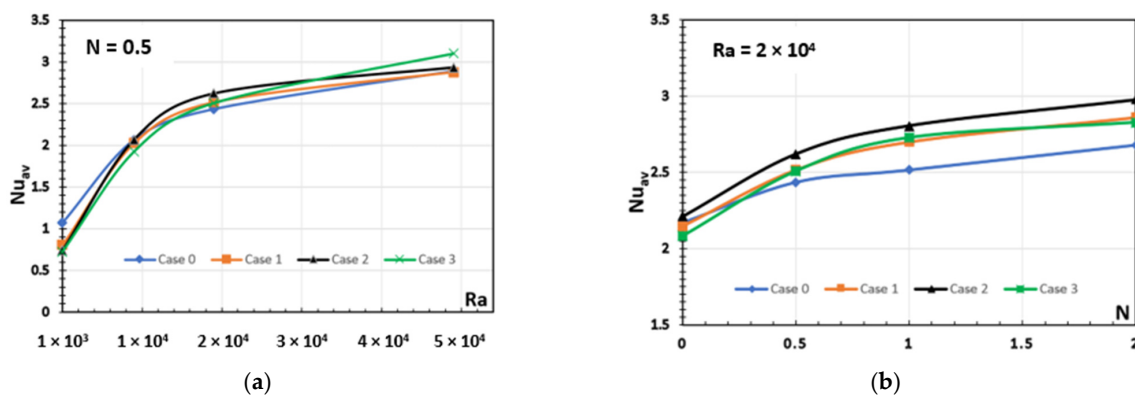


Figure 7. Effect of Rayleigh number (a) and buoyancy ratio for $Ra = 2 \times 10^4$ (b) on the average heat transfer rate in all cases for $\theta = 0^\circ$.

Figure 7b shows the effect of buoyancy rate on the average heat transfer rate in all cases studied for $Ra = 2 \times 10^4$ and $\theta = 0^\circ$. The average heat transfer rate rises with increasing N . The thermal and solutal buoyancy forces cooperate for positive values of the buoyancy ratio. From $N = 0.5$, the average heat transfer rate is highest in case 2. When N is greater than 1, a 12% improvement in the average heat transfer rate compared to the reference case is observed. Cases 1 and 3 have almost equal average Nusselt values with a 6% improvement over the reference case.

Figure 8a illustrates the effect of Rayleigh numbers on the average mass transfer rate in all cases for $N = 0.5$ and $\theta = 0^\circ$. The average mass transfer rate increases with the Rayleigh number. Case 3 has the lowest average Sherwood values for all Rayleigh numbers studied. From $Ra = 10^4$, cases 0 and 1 have nearly equal mass transfer rate values and are the highest compared to the other cases.

The effect of the buoyancy ratio on the average mass transfer rate for $Ra = 2 \times 10^4$ and $\theta = 0^\circ$ is shown in Figure 8b. Case 3 displays the minimum values of the average Sherwood for all values of N . Cases 0 and 2 exhibit the maximum values of the mass transfer rate with approximately equal values. When the buoyancy ratio is changed from $N = 0$ to 2, a significant enhancement of about 150% is seen for all cases studied.

Figure 9a shows the effect of the tilt of the solar panel on the average heat transfer rate for $Ra = 5 \times 10^4$, $N = 0$, and $N = 1$. When $N = 0$, for the reference case, inclination

caused a decrease in the average heat transfer rate. From $\theta = 0^\circ$ to $\theta = 10^\circ$, a decrease of 12% is observed. The average Nusselt number shows constant values in the range of 10° to 20° , then undergoes another decrease of 10% from $\theta = 25^\circ$. When the inclination is less than 18° , all cases studied have higher average Nusselt values than the reference case. And case 2 has higher values of average heat transfer rate. When $N = 1$, the evolution of the average Nusselt as a function of the inclination presented is completely different from that of $N = 0$. Indeed, the heat transfer rate for cases 1,2, and 3 is higher than the reference case only when θ is lower than 5° . A considerable decrease of 45% of the average transfer rate is observed for these three cases when moving from $\theta = 5^\circ$ to $\theta = 10^\circ$ while it is 10% for the reference case.

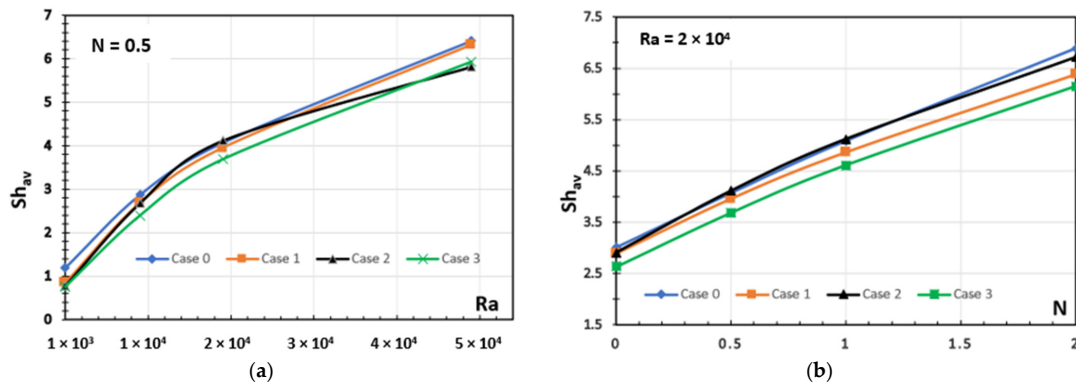


Figure 8. Effect of Rayleigh number (a) and buoyancy ratio for $Ra = 2 \times 10^4$ (b) on the average mass transfer rate in all cases for $\theta = 0^\circ$.

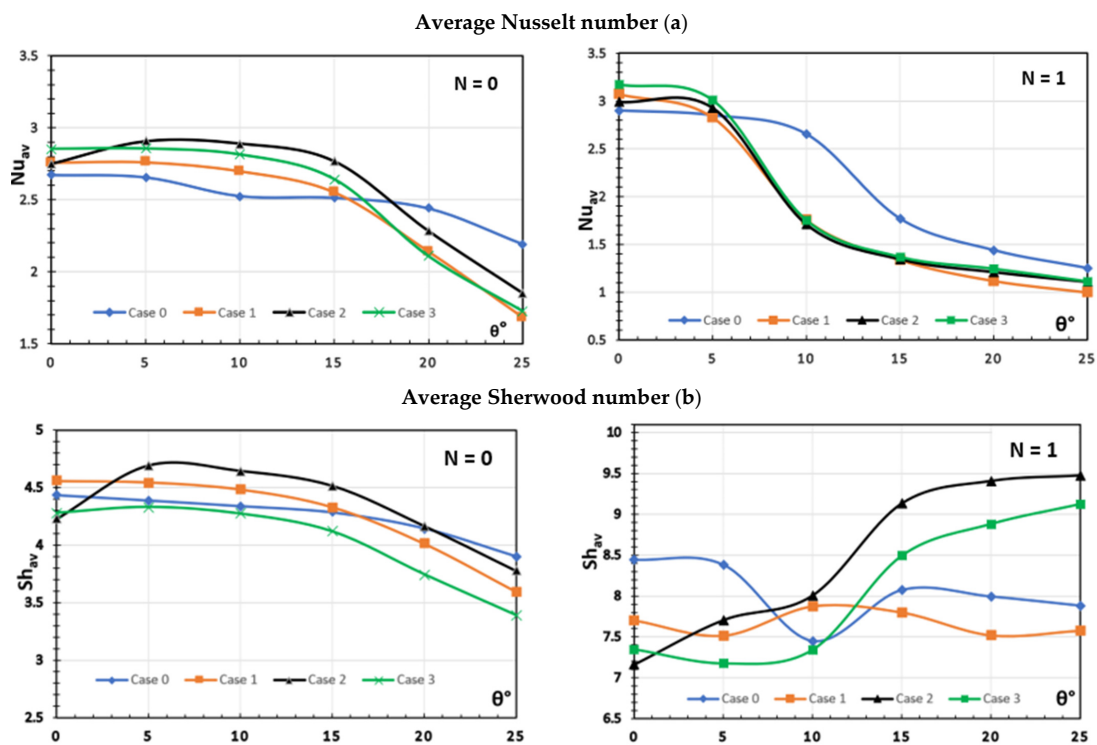


Figure 9. Effect of inclination on the average Nusselt (a) and Sherwood (b) in the all cases for $Ra = 5 \times 10^4$, $N = 0$ and $N = 1$.

Figure 9b presents the effect of the tilt on the average mass transfer rate when $Ra = 5 \times 10^4$, $N = 0$ and $N = 1$. When $N = 0$, for cases 0 and 1, the increase of the tilt angle decreases the average Sherwood. For cases 2 and 3, the evolution is parabolic with

a maximum of the average transfer rate observed for $\theta = 5^\circ$. For all angles studied, the average mass transfer rate for case 3 is the lowest of the cases. In the range of angles between 5° and 20° , case 2 has the highest average mass transfer rate.

When $N = 1$, the trend in the averages of Sherwood for the reference case shows a minimum at $\theta = 10^\circ$. When θ is less than 8° , the reference case shows the highest values compared to the other cases, but between 8° and 13° , it shows the lowest values. Cases 2 and 3 exhibit higher average Sherwood values than the reference case from $\theta = 12^\circ$. Increasing the angle from 0° to 25° exhibits for case 2 an increase in the average mass transfer rate of 35%.

4.3. Sensitivity Analysis

The sensitivity analysis is performed based on two response variables and four factors. The response variables are respectively the mean values of the Nusselt number and the Sherwood number. The model factors are the Rayleigh number Ra , the buoyancy ratio N , the baffle design, and the tilt angle of the solar still.

The minimum and maximum level of each factors were: $Ra = [10^3, 5 \times 10^4]$, $N = [0, 2]$ and $\theta = [0, 25^\circ]$. For the baffle design factor, four configurations were performed and labeled as 0: reference case, 1: plane, 2: triangular, and 3: curvilinear.

The regression equations for mean Nusselt and Sherwood respectively are as follows:

$$Nu_{av} = 0.647 + 1.31 \times Ra - 0.247 \times N - 0.0738 \times \text{Baffle design} - 0.152 \times \theta$$

$$Sh_{av} = -3.38 + 4.18 \times Ra + 1.38 \times N - 0.666 \times \text{Baffle design} - 0.0835 \times \theta$$

The regression equation shows that the average Nusselt number is too much influenced by the Rayleigh number, the buoyancy ratio N , and the inclination angle. While the baffle design has the least impact.

Regarding the regression equation for the average Sherwood number, it can be seen that the Rayleigh number, the buoyancy ratio N , and the baffle design have the most important impact.

The estimated R^2 value of the heat transfer rate model was 92.5% while that of the mass transfer rate model was 87.8%.

5. Conclusions

The effect of the inclination on the double-diffusive convection in pyramid-shaped floating solar still filled with air vapor ($Le = 0.85$ and $Pr = 0.7$) was numerically investigated. Four different configurations of baffles mounted in the cooling region were studied. Case 0 is considered as a reference case, case 1 is a flat baffle, case 2 is triangular, and case 3 is curvilinear in shape. A parametric study was performed as a function of Rayleigh number, buoyancy ratio, and the angle of inclination of the floating still. The main conclusions are as follows:

- Uncooled air-vapor leakage was observed during tilting for the solar still equipped with a small flat baffle (reference case) at the cooling zone.
- The triangular and curvilinear baffle design assisted the air-vapor mixture to cool down before the exit.
- When $Ra = 2 \times 10^4$ and $\theta = 0^\circ$, from $N = 0.5$, the average heat transfer rate is highest in case 2, for triangular baffle. A 12% improvement in the average heat transfer rate compared to the reference case is observed.
- When $Ra = 5 \times 10^4$ and $N = 0$, an improvement of the air-vapor convection is observed in the heating zone for all the new baffles designs studied at $\theta = 15^\circ$. The thermal gradient is enhanced in the cooling zone mainly in the middle of the cold surfaces for cases 2 and 3. When the inclination is less than 18° , all cases studied have higher average Nusselt values than the reference case. And case 2 has higher values of average heat transfer rate. For cases 2 and 3, triangular and curvilinear baffle design, the evolution is parabolic with a maximum of the average transfer rate observed for

$\theta = 5^\circ$. In the range of angles between 5° and 20° , case 2 has the highest average mass transfer rate.

- When $Ra = 5 \times 10^4$ and $N = 1$, the heat transfer rate for cases 1, 2, and 3 is higher than the reference case only when θ is lower than 5° . Cases 2 and 3 exhibit higher average Sherwood values than the reference case from $\theta = 12^\circ$. Increasing the angle from 0° to 25° exhibits for case 2 an increase in the average mass transfer rate of 35%.

Finally, the design of a triangular baffle mounted in the cooling region is highly recommended to improve the thermal and mass performance of the floating solar still.

Author Contributions: Literature review and thermal modeling, M.A.A.; Development of the numerical code, Analysis, discussion, and interpretation of results, C.M. All authors have read and agreed to the published version of the manuscript.

Funding: This research was funded by the Deanship of Scientific Research, Imam Mohammad Ibn Saud Islamic University, Saudi Arabia, grant number 19-12-14-001.

Institutional Review Board Statement: Not applicable.

Informed Consent Statement: Not applicable.

Data Availability Statement: Not applicable.

Acknowledgments: This research was supported by the Deanship of Scientific Research, Imam Mohammad Ibn Saud Islamic University, Saudi Arabia, Grant No. (19-12-14-001).

Conflicts of Interest: The authors declare no conflict of interest.

Nomenclature

C	Dimensionless concentration
D	Mass diffusivity (m^2/s)
Gr	Grashof number
K	Thermal conductivity ($W/m \cdot K$)
H	Height from the base surface to the top (m)
L	Baffle width (m)
Le	Lewis number
N	Buoyancy ratio
Nu	Nusselt number
Pr	Prandtl number
Ra	Rayleigh number
Sh	Sherwood number
T	Dimensionless time ($=t' \cdot \alpha / H^2$)
T	Dimensionless temperature
\vec{V}	Dimensionless velocity vector ($=\vec{V}' \cdot H / \alpha$)
Greek symbols	
α	Thermal diffusivity (m^2/s)
β_t	Coefficient of thermal expansion (K^{-1})
β_c	Coefficient of solutal expansion (K^{-1})
μ	Dynamic viscosity ($kg/m \cdot s$)
ν	Kinematics viscosity (m^2/s)
$\vec{\psi}$	Dimensionless vector potential ($\vec{\psi}' / \alpha$)
$\vec{\omega}$	Dimensionless vorticity ($=\vec{\omega}' \cdot \alpha / H^2$)
Θ	Angle of inclination of still
Subscripts	
x, y, z	Cartesian coordinates
h	hot, high
c	Cold
l	Low
av	average
0	reference

References

1. Ghachem, K.; Kolsi, L.; Mâatki, C.; Hussein, A.K.; Borjini, M.N. Numerical simulation of three-dimensional double diffusive free convection flow and irreversibility studies in a solar distiller. *Int. Commun. Heat Mass Transf.* **2012**, *39*, 869–876. [[CrossRef](#)]
2. Sathyamurthy, R.; Harris Samuel, D.G.; Nagarajan, P.K.; Arunkumar, T. Geometrical variations in solar stills for improving the fresh water yield—A review. *Desalination Water Treat.* **2016**, *57*, 1944–3986. [[CrossRef](#)]
3. Rahbar, N.; Asadi, A.; Fotouhi-Bafghi, E. Performance evaluation of two solar stills of different geometries: Tubular versus triangular: Experimental study, numerical simulation, and second law analysis. *Desalination* **2018**, *443*, 44–55. [[CrossRef](#)]
4. Al-Madhhachi, H.; Smaism, G.F. Experimental and numerical investigations with environmental impacts of affordable square pyramid solar still. *Sol. Energy* **2021**, *216*, 303–314. [[CrossRef](#)]
5. Moussa, R.R.; Hatem, T.M. Estimating the potential of desalinate seawater using solar glass pyramid (SGP) in hot arid zones. *Clean. Eng. Technol.* **2021**, *4*, 100189. [[CrossRef](#)]
6. Kabeel, A.E.; Abdelgaied, M. Enhancement of pyramid-shaped solar stills performance using a high thermal conductivity absorber plate and cooling the glass cover. *Renew. Energy* **2020**, *146*, 769–775. [[CrossRef](#)]
7. Xiong, J.; Xie, G.; Zheng, H. Experimental and numerical study on a new multi-effect solar still with enhanced condensation surface. *Energy Convers. Manag.* **2013**, *73*, 176–185. [[CrossRef](#)]
8. Dev, R.; Tiwari, G.N. Characteristic equation of a passive solar still. *Desalination* **2009**, *245*, 246–265. [[CrossRef](#)]
9. Sebastian, G.; Shah, A.; Thomas, S. The effect of vapour space temperature on the productivity of a passive solar still integrated with multi-functional floating absorber. *J. Water Process Eng.* **2021**, *44*, 102349. [[CrossRef](#)]
10. Kaushal, A.K.; Mittal, M.K.; Gangacharyulu, D. An experimental study of floating wick basin types vertical multiple effect diffusion solar still with waste heat recovery. *Desalination* **2017**, *414*, 35–45. [[CrossRef](#)]
11. Ni, G.; Zandavi, S.H.; Javid, S.M.; Boriskina, S.V.; Cooper, T.A.; Chen, G. A Salt-Rejecting Floating Solar Still for Low-Cost Desalination. *Energy Environ. Sci.* **2018**, *11*, 1510. [[CrossRef](#)]
12. Wang, Q.; Zhu, Z.; Zheng, H. Investigation of a floating solar desalination film. *Desalination* **2018**, *447*, 43–54. [[CrossRef](#)]
13. Chen, S.; Zhao, P.; Xie, G.; Wei, Y.; Lyu, Y.; Zhang, Y.; Yan, T.; Zhang, T. A floating solar still inspired by continuous root water intake. *Desalination* **2021**, *512*, 115133. [[CrossRef](#)]
14. Alvarado-Juárez, R.; Álvarez, G.; Xamán, J.; Hernández-López, I. Numerical study of conjugate heat and mass transfer in a solar still device. *Desalination* **2013**, *325*, 84–94. [[CrossRef](#)]
15. Alvarado-Juárez, R.; Xamán, J.; Álvarez, G.; Hernández-López, I. Numerical study of heat and mass transfer in a solar still device: Effect of the glass cover. *Desalination* **2015**, *359*, 200–211. [[CrossRef](#)]
16. Ghachem, K.; Maatki, C.; Kolsi, L.; Alshammari, N.; Oztop, H.F.; Borjini, M.N.; Ben, A.H.; Al-Salem, K. Numerical study of heat and mass transfer optimization in a 3-d inclined solar distiller. *Therm. Sci.* **2017**, *21*, 2469–2480. [[CrossRef](#)]
17. Maatki, C. Heat transfer enhancement using CNT-water nanofluids and two stages of seawater supply in the triangular solar still. *Case Stud. Therm. Eng.* **2022**, *30*, 101753. [[CrossRef](#)]
18. Subhani, S.; Kumar, R.S. Numerical investigation on influence of mounting baffles in solar stills. In Proceedings of the AIP Conference Proceedings, Tamil Nadu, India, 14–15 March 2019; Volume 2161, p. 020025. [[CrossRef](#)]
19. Edalatpour, M.; Kianifar, A.; Ghiami, S. Effect of blade installation on heat transfer and fluid flow within a single slope solar still. *Int. Commun. Heat Mass Transf.* **2015**, *66*, 63–70. [[CrossRef](#)]
20. Serradj, D.B.; Anderson, T.N.; Nates, R.J. The use of passive baffles to increase the yield of a single slope solar still. *Sol. Energy* **2021**, *226*, 297–308. [[CrossRef](#)]
21. Maatki, C. Three-Dimensional Numerical Study of the Effect of Protective Barrier on the Dispersion of the Contaminant in a Building. *Mathematics* **2021**, *9*, 1125. [[CrossRef](#)]
22. Patankar, S.V. *Numerical Heat Transfer and Fluid Flow*; Taylor & Francis: Philadelphia, PA, USA, 1981.
23. Ghachem, K.; Hassen, W.; Maatki, C.; Kolsi, L.; Al-Rashed, A.A.; Naceur, M. Numerical simulation of 3D natural convection and entropy generation in a cubic cavity equipped with an adiabatic baffle. *Int. J. Heat Technol.* **2018**, *36*, 1047–1054. [[CrossRef](#)]
24. Rahman, M.M.; Öztop, H.F.; Ahsan, A.; Kalam, M.A.; Varol, Y. Double-diffusive natural convection in a triangular solar collector. *Int. Commun. Heat Mass Transf.* **2012**, *39*, 264–269. [[CrossRef](#)]